IEEE Access
Multidisciplinary ⋮ Rapid Review ⋮ Open Access Journal

Received 10 April 2024, accepted 7 May 2024, date of publication 15 May 2024, date of current version 24 May 2024.

Digital Object Identifier 10.1109/ACCESS.2024.3401472

RESEARCH ARTICLE

Development of a Real-Time Geometric Quality Monitoring System for Extruded Filaments of 3D Concrete Printing Construction

JIHYE JHUN, DONG-HYUN LEE, ATTA UR REHMAN, SEUNGWOO KANG, AND JUNG-HOON KIM

Department of Civil and Environmental Engineering, Yonsei University, Seoul 03722, South Korea

Corresponding author: Jung-Hoon Kim (junghoon@yonsei.ac.kr)

This work was supported by the National Research Foundation (NRF) Korea under Grant NRF-2021R1A2C2013522.

ABSTRACT Extrusion-based 3D concrete printing (3DCP) is an additive manufacturing (AM) technology in the construction field and is gaining significant attention as an emerging construction method for the future. The variability in concrete composite material properties in this field poses a challenge in maintaining consistent printing quality. Furthermore, the economic and environmental costs of discarding large structures in case of printing failures are significantly higher compared to other AM technologies. These inherent characteristics highlight the critical need for real-time, in-situ quality monitoring of printed filaments during the 3DCP process. Existing studies on geometric quality monitoring techniques provide only partial information on the extruded concrete filaments, such as width or height, and some studies are limited to linear paths. Moreover, the requirements of 3DCP, such as cost, weight, installation space, minimum object distance (MOD), field of view (FOV), and maintenance, make it challenging to find suitable commercial 2D laser profile sensors. Therefore, this paper presents the design of a 2D profile sensing system tailored to meet the requirements of 3DCP and proposes an algorithm that can compute comprehensive cross-sectional information, including the width, thickness, and area of the extruded concrete filament during 3D printing. Notably, the proposed sensing system is integrated with an infinitely rotatable nozzle device on the end effector of a 3D printer robot arm, enabling continuous monitoring of extrusion in all directions along the printing path. Comprehensive experimental results from static, motion, and concrete 3D printing tests validate that the developed 2D profile sensing system is capable of performing real-time, in-situ quality monitoring in 3DCP by accurately computing filament cross-sectional shape information. Furthermore, this paper provides a comprehensive solution that includes practical calibration method along with design, offering a crucial technology for detecting defects and failures, ultimately contributing to the high-quality and safe construction of structures in 3DCP.

INDEX TERMS 2D laser profile sensor, 3D concrete printing, extrusion monitoring, geometrical accuracy, print quality.

I. INTRODUCTION

3D Concrete Printing (3DCP) or additive manufacturing construction is a rapidly advancing construction method that has gained enormous popularity in the last decade [1]. In this method, the design of the desired object is created in computer-aided design (CAD) software. Once the design is ready, it is converted into a format that can be understood by the concrete printer. This conversion process, called slicing, takes into account the cross-sectional dimensions of the printer nozzle and divides the CAD model of the object into thin layers which are compatible with the size of the printer nozzle. The slicing software generates a set of instructions called "G-code" which guides the printing

The associate editor coordinating the review of this manuscript and approving it for publication was Zhiwu Li.

path of the 3D printer nozzle for each layer of the object. The G-code is transferred to the concrete printer, which starts manufacturing the object by depositing concrete layer by layer [2]. 3DCP is an automated construction process that does not use formwork for construction. This technology has the potential to reduce construction time and cost, minimize construction material wastage and enable the fabrication of complex concrete structures with greater design freedom [3].

For 3DCP construction, concrete material is produced by mixing ingredients with water, which is then pumped to the printer nozzle. The nozzle extrudes the concrete along the pre-defined print path according to G-code, as shown in Fig. 1. During the extrusion phase, fresh concrete is printed onto the print bed in the desired shape using a customized nozzle with a specified cross-sectional area. Rectangular-shaped nozzles are preferred over circular cross-sectional ones in 3DCP construction because they can provide better stability and surface finish [4]. Hence, this study utilized a rectangular nozzle. During 3D concrete printing, the extruded concrete layers are compressed by upper layers, and each layer should be able to retain its dimensions and rectangular shape in order to successfully attain a three-dimensional object as specified in the digital model. Over-extrusion or under-extrusion can occur when the properties of the printing material change or when there is a lack of synchronization between the concrete extrusion rate and the nozzle traveling speed [5]. Over-extrusion can produce a thicker printed concrete object than the designed object, and under-extrusion can lead to a thinner and weaker object. The geometrical inaccuracy of printed concrete filament can also lead to print failure [6]. Therefore, the geometric conformability between the extruded concrete layer and the designed object is crucial. However, achieving perfect conformability is a challenging task due to the influence of multiple parameters, such as the quality of concrete used for 3D printing, nozzle speed, extrusion rate, nozzle stand-off distance (the gap between the nozzle and the print bed or previous concrete layer), ambient temperature, and humidity [7]. If the printing nozzle velocity is not synchronized with the extrusion rate or the quality of the concrete material is poor, it negatively impacts the geometric quality of the extruded concrete [8]. Similarly, improper nozzle stand-off distance and changes in temperature and humidity affect the geometrical quality of extruded concrete [1]. This necessitates robust and real-time monitoring of the geometry of extruded concrete layers and ensuring the desired quality by taking necessary actions such as an adjustment in concrete feeding rate, nozzle velocity, nozzle stand-off distance, concrete quality, etc. [9].

During 3DCP construction, the printing quality of extruded concrete layers is determined by its dimensional conformity and consistency [10]. However, when fresh concrete with low shape stability is produced, deformation of the layers often occurs during printing. Consequently, monitoring and managing the shape of the printed layers become necessary to achieve better printing quality. Currently, most of the 3DCP construction industry measures the shape information

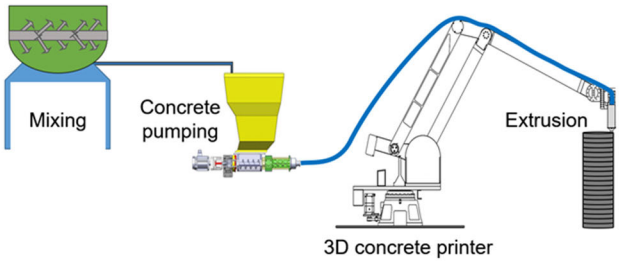

FIGURE 1. Overview of the 3D concrete printing process [11].

TABLE 1. Overview of prior studies related to quality monitoring in the 3DCP construction.

Printing method	Sensor	Data dimension & type	Measured or computed value	Printing path	Ref.
Material extrusion	Time of flight (ToF) distance sensor	1D single point data	Height of layer	Linear	[12]
Material extrusion	Depth sensor	3D point cloud data	Distance between nozzle to the surface	Linear	[13]
Material extrusion	Single camera	2D image data	Layer width	Linear	[14], [19]
Shotcrete (Spraying)	Laser triangulation	2D profile data	Layer width, Layer height	Linear wall	[15]
Other (Welding)	Laser triangulation	2D profile data	2D profile	Linear	[16]
Material extrusion	Two cameras : It is not a stereo camera	2D image data	Layer width	Linear, Curved	[17]
Material extrusion	Laser triangulation	2D profile data	Layer width, Layer height, Layer area	Linear, Curved	Proposed system in this paper

(width, height) of extruded concrete layers manually using instruments such as vernier calipers or rulers during printing. While manual measurement is simple, it is time-consuming, labor-intensive, and prone to human errors and accidents, particularly when there is a risk of collision between a moving nozzle and a worker. Therefore, there is a need for advanced, reliable, automated, and safe techniques for measuring the geometric quality of extruded concrete. Recognizing the need for innovative geometric quality monitoring techniques in 3DCP construction, this research contributes by developing a sensing system for measuring the width, height, and cross-sectional area of the extruded layers. This system possesses the following characteristics:

- Automated inline testing
- Real-time testing
- Non-contact and non-destructive testing
- Digital testing
- Economical testing

II. LITERATURE REVIEW

Previous researchers have focused on the development of automated systems for the geometrical quality inspection and assurance of the printed concrete layers. These studies, summarized in Table 1, are critically discussed in the following lines.

Wolfs et al. [12] presented a real-time height control method for 3DCP using a real-time distance sensor based on time of flight (ToF). The 1D laser distance sensor transmitted the measured nozzle stand-off distance (single point data) to the control unit, which maintained the specified nozzle height. This system enabled the printer to adjust its nozzle height to compensate for the altered nozzle stand-off distance due to the deformations in the previously printed layers. In this way, negative effects on the geometric quality of extruded layers due to variations in nozzle stand-off distance and deformation in the previously deposited concrete layers could be minimized. However, in this study, the nozzle stand-off distance was calculated for a one-dimensional point where the laser pointer was indicated. For better accuracy and robust control over the geometric quality, sensors with the potential to capture a 2D or 3D profile of the concrete layer should be used in such feedback systems. Lee [13] proposed a method to reliably measure the nozzle stand-off distance to the concrete layer through spatiotemporal processing of 3D point cloud data from a depth sensor, and used it to implement an advanced nozzle gap feedback system. However, depth sensors have limitations when it comes to accurately measuring the cross-sectional shape of extruded concrete filaments with sub-millimeter accuracy. Kazemian et al. [14] proposed the application of computer vision for real-time monitoring of the width of extruded concrete layer. The proposed system involved using a 2D image from a single camera installed near the printer nozzle to capture the width of the printed concrete layer, assuming a constant distance from the camera to the top surface of the extruded layer; the captured images were analyzed using an algorithm to detect the scenarios of over-extrusion and under-extrusion. Although the system was automated, it could not measure the height and cross-section area of the extruded concrete layers. Moreover, the height of the layer was assumed to be constant to calculate the extrusion rate in this study, but accurate quality monitoring procedure require height measurements. Lindemann et al. [15] developed a multi-loop control system to enhance the geometrical accuracy of concrete elements produced by spray-based shotcrete 3D printing. The developed controller sensed the inaccuracies using the 2D profile data collected by the laser triangulation system and attempted to minimize the production defects and increase the robustness of the shotcrete 3D printing. However, this approach was developed for shotcrete 3D printing, and it had the limitation of detecting the shape of the extruded filament layer in a curved printing path since the sensor could not be rotated relative to the extrusion nozzle and concrete hose. Additionally, extrusion-based 3DCP is different from shotcrete 3D printing due to the layer-wise extrusion of concrete rather than the spraying of concrete; hence application of a laser triangulation system for extrusion-based 3DCP should be established. Moreover, the use of the rotatable nozzle is necessary to acquire profile data in a curved printing path, as adopted in this study. A similar study from the aspect of laser welding has been conducted by Huang and Kovacevic [16] using a vision sensor based on the principle of laser triangulation to inspect the weld quality and detect the presence of various weld defects. A visual analysis of the acquired 3D profiles of the welding surface was performed after collecting 2D image data. Extension of such approaches from contemporary fields of welding to 3DCP construction can be helpful. However, the defects in 3D-printed concrete layers are different from welding defects, and the potential of laser triangulation for detecting the quality of 3D-printed concrete should be carefully investigated. Furthermore, a vision system based on a deep learning algorithm for detecting the concrete filament width and adjusting the nozzle speed to maintain a fixed width was reported in [17]. In this system, two cameras were attached to the left and right sides of the nozzle to acquire 2D image data and monitor the extrusion of the filament around it. However, it could not obtain depth information using the stereo camera principle because the nozzle obstructed the field of view between the two cameras. The purpose of introducing two cameras here was to simply monitor the extrusion of the filament in all directions around the nozzle as it moved. Therefore, the system had to make assumptions about the height information of the filament. Even if a stereo camera were used, the feature detection when moving in different views during the printing process might not be accurate because the stereo camera may camouflage the true matches due to false matches between the images [18]. In summary, this method can determine only the width of the printed layers, while it cannot ascertain the height and cross-sectional area of the printed filament. Recently, Barjuei et al. [19] proposed a vision-based feedback control system to maintain the fixed layer width for printing rectangular-shaped concrete layers. In this system, the layer width is calculated using an edge detection algorithm applied to the 2D image data obtained from a camera. By considering the three factors; nozzle dimensions, feeding rate of concrete, and top view of the rectangular extruded layers, this system ensured the specified width of extruded layers by manipulating the print speed without changing the pump flow rate. This proposed system is a swift and automatic method; however, the response of this system to printable concrete with low shape retention capability is unknown. The concrete may laterally deform due to lower shape retention capability, which might be considered by this system as over-extrusion. Additionally, this system has the limitation of measuring the height and cross-sectional area of extruded layers.

The above literature regarding the use of automated geometric quality control shows that the previous research studies have predominantly focused either on the nozzle stand-off distance or the width of the printed concrete filament. However, the measurement of nozzle stand-off distance does not give enough information for calculating the cross-sectional geometry of the printed concrete layer. Additionally, the printed layer may not have a perfect rectangular-shaped cross-section. Therefore, the calculated cross-sectional area solely based on a single measurement (width of filament) may not reflect the real cross-sectional

area of the deposited concrete layer. Hence, there is a clear need for the development of geometric quality sensing systems that can measure the real-time width, height, and cross-sectional area of the printed concrete [20]. By encompassing these comprehensive measurements, such systems can provide a more accurate representation of the geometric quality of the printed concrete layers.

It should be noted that the camera-based machine learning methods with Convolutional Neural Network (CNN) or object detection model has shown effectiveness in classifying anomalies in print quality during the printing process. Jin et al. [21] established an anomaly detection system using a CNN model for the 2D camera image data to recognize anomalies in the 3D bioprinting process by classifying three imperfections: discontinuity, irregularity, and nonuniformity of bioprinted materials. Goh et al. [22] developed a real-time monitoring system based on YOLOv3-Tiny that detects and classifies printing anomalies, including under-extrusion and over-extrusion, in the Fused Filament Fabrication (FFF) process with an accuracy of 89.8% from a total dataset of 18,000 samples. As part of an in-process closed-loop feedback system, corrective actions were performed to increase the material flow rate when under-extrusion was detected and to reduce it when over-extrusion was detected. This study showcased the capability to move beyond the traditional binary classification of 'defective' and 'non-defective' outcomes in machine learning methods towards correcting printing defects within an in-situ monitoring system. Fu et al. [23] fabricated dog-bone specimens using a desktop Fused Deposition Modeling (FDM) 3D printer with polylactic acid filament, while varying the length and location to create 30 classes of void defects. They employed a CNN model to classify the length and location of defects, achieving an average accuracy of 99.78% and an F1-score of 99.57% using a dataset consisting of 1550 augmented images. Additionally, they introduced a real-time system for assessing the structural quality of specimens using Support Vector Machine (SVM)-based decision-making technique with additional tensile test data (comprising 450 samples, including 221 defect cases) on the specimens. This study represents an important step forward in exploring the potential of applying machine learning to structural validation. However, the authors also acknowledged a key drawback, namely the significant time and effort required to obtain mechanical performance data through tensile tests. Furthermore, in the field of 3D concrete printing, there is a complex and challenging issue that necessitates consideration: the rapid changes in fresh properties over several hours after extrusion, in addition to the hardened properties after one month [1]. Thus, acquiring a vast amount of data to enable structural performance evaluation is extremely challenging and not practical in the field of 3D concrete printing.

The decision to utilize image processing techniques with the 2D laser profile data over these advanced machine learning approaches in the context of 3D concrete printing is based on several critical considerations unique to the construction site. One of the main reasons is the inherent variability of concrete material properties, which can be significantly influenced by environmental factors such as temperature and humidity. This presents unique challenges in data collection for machine learning, necessitating extensive datasets that accurately represent a wide range of printing conditions and anomalies unlike simpler processes such as plastic fused deposition modeling. Plastic and metal printing processes are characterized by material properties that are relatively less affected by daily fluctuations in temperature and humidity, and they are mostly carried out under indoor environmental conditions where these variations can be controlled. These materials involve a highly controllable printing process during which they melt at specific temperatures and rapidly solidify within seconds, facilitating the creation of large datasets for machine learning applications. Similarly, in the context of automated machine learning based monitoring of sport such as badminton [24], acquiring a dataset comprising hundreds of shots can be readily accomplished by recording a single game between players. This scenario stands in stark contrast to the challenges faced in 3D concrete printing (3DCP) construction projects, where collecting comparable datasets is significantly more complex and very costly. The variability of concrete material and the limited controllability of the 3DCP process, combined with the changes in concrete properties over time, add further complexity to controlled data collection, making it intricate and resource-intensive, demanding significant time, cost, and effort. There are also challenges in machine learning-based approaches for precise geometrical output in 3D concrete printing. Although state-of-the-art machine learning methods have recently been applied in the 3D printing field, these data-driven approaches need further research for producing the exact geometrical values required for real-time feedback. Currently, the limitations may arise from the limited resolution of the output and the high cost of collecting extensive datasets, especially in 3DCP.

This paper employs an image processing method to extract information from 2D profile data derived from images, facilitating the calculation of cross-sectional shape information. This approach enables the direct application of customized algorithms tailored to accurately calculate the geometric characteristics of the extruded filament, ensuring real-time and reliable performance without the need for extensive datasets. Additionally, it offers computational efficiency, making it deployable on lighter hardware without a Graphics Processing Unit (GPU) and ensuring scalability across various printing setups.

To address the need for enhanced geometric quality control in 3DCP, this study introduces a real-time monitoring system based on 2D laser profile sensing. The system can evaluate object profiles with an impressive accuracy of 0.067mm and proposes processing algorithms capable of calculating all geometric parameters, including width, thickness, and cross-sectional area of printing layers, in real-time from camera images.

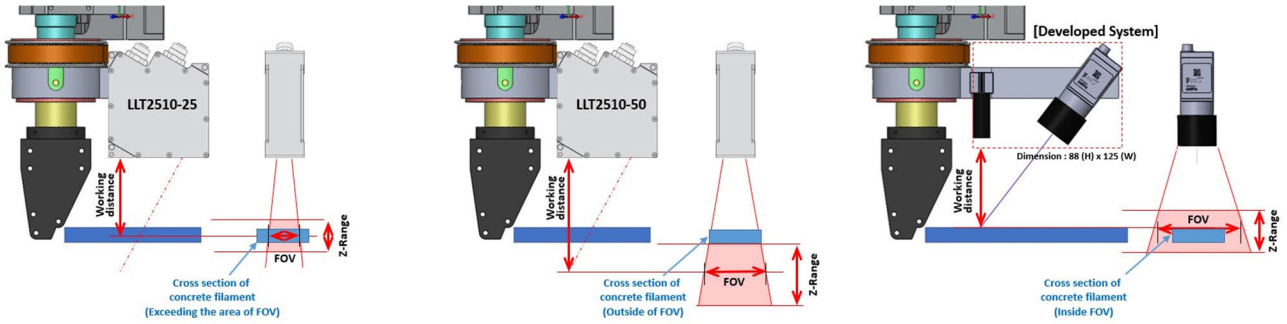

FIGURE 2. Working distance, FOV of 2D profile detection sensors when installed to the printing nozzle of 3DCP robot. (a) LLT2510-25. (b) LLT2510-50. (c) Developed system.

TABLE 2. Comparison of commercially available sensors and the developed 2D profile sensing system, and suitability to design requirements (FOV = 70 mm × 35 mm, WD = 69mm).

Model with Manufacturer	Cost (US dollar)	X resolution	FOV (X-axis)	Z-axis Range	Working distance	Dimension (H×W×D)	Weight
LJ-8080 (Keyence)	13,500 with LJ-X8000A controller	12.5 µm	35 mm	41 mm	73 mm	108×145×57 mm	1,100 g
LJ-8200 (Keyence)	13,500 with LJ-X8000A controller	25 µm	72 mm	68 mm	245 mm	108×185×55 mm	1,200 g
LJ-V7080 (Keyence)	9,000 incl. XG-X2802LJ controller	50 µm	32 mm	46 mm	80 mm	71×96×42 mm	400 g
LJ-V7200 (Keyence)	9,000 incl. XG-X2802LJ controller	100 µm	62 mm	96 mm	200 mm	77×145×42 mm	550 g
LLT2510-25 (Micro-epsilon)	7,500	40 µm	25 mm	25 mm	66 mm	96×85×33 mm	380 g
LLT2510-50 (Micro-epsilon)	7,500	80 µm	50 mm	50 mm	95 mm	96×85×33 mm	380 g
LLT2510-100 (Micro-epsilon)	7,500	16 µm	100 mm	100 mm	240 mm	96×85×33 mm	380 g
Developed System	875	80 µm	70 mm	35 mm	69 mm	88×125×35 mm	234 g

There are commercially available sensors for 2D profile scanning. Table 2 lists commercial sensors and a comparative analysis between them and the developed 2D profile sensing system, showing cost, resolution, FOV, Z-axis range, working distance, dimensions, and weight measurements. Commercial sensors and the developed sensor operate on the principle of laser triangulation. The developed sensor consists of a 2D line laser and a CCD camera, the commercial sensors also consist of a lens and CCD device. However, commercial sensors are unsuitable for 3DCP due to their high cost, maintenance costs associated with contamination, minimum object distance (MOD), size, limited field of view (FOV), and challenges in replacement. Replacing contaminated commercial sensors in construction site environments where contamination is inevitable often entails significant costs and logistical challenges. As shown in Table 2, finding commercial sensors that meet the requirements of 3D concrete printers is challenging. Notably, while commercial sensors require a minimum of $7,500 USD, the developed sensor costs less than $1,000 USD, representing only a fraction of the cost of commercial sensors. Therefore, this study develops a low-cost sensor that is finely crafted to meet specified working distance, FOV, and size specifications. The sensor seamlessly integrates with the robotic arm of a 3D concrete printer and can be easily replaced. Furthermore, the developed system boasts a lighter weight than commercial sensors and enhances nozzle movement. Additionally, the developed sensor is integrated with a rotatable nozzle, which allows quality monitoring of printed concrete for both linear and curved shapes. Also, the proposed processing algorithm for a 2D profile sensing system is customized for the 3D concrete printer. Moreover, the algorithm can calculate the extruded concrete's width, height, and cross-sectional area.

Fig. 2 compares the working distance and FOV when integrating the developed sensor and commercial sensors with a 3D concrete printer. The black area represents the printing nozzle, the large blue rectangle denotes the printed concrete layer, and the small blue rectangle represents the cross-section of the printed concrete layer. In Fig. 2(a), sensor LLT2510-25 is attached to the robotic arm of the 3D concrete printer, specifically to the printing nozzle section. However, the sensor's working distance extends beyond the surface of the concrete layer, and its FOV does not encompass the entire cross-section, making it unsuitable for accurate detection. In Fig. 2(b), sensor LLT2510-50 is attached to the robotic arm. However, it has an excessively long working distance

and a FOV that does not cover the entire cross-section of the printed concrete, making accurate detection impossible. In contrast, Fig. 2(c) shows that the developed sensing system maintains an accurate working distance from the surface of the printed concrete and has a sufficiently large FOV to cover the entire cross-section. This strategic positioning ensures precise data capture.

Furthermore, the developed device offers operational advantages in research and development efforts in 3DCP technology. It provides detailed calibration, operational, and application insights on material printing performance. Concrete printing robots' functionality can be improved to enhance real-time feedback control, and innovations in printing materials are also being pursued to enhance concrete printing characteristics. Leveraging the precision of the new sensor, a feedback system synchronizing concrete materials mix design and printing parameters is being developed to optimize the printing process. Future work involves converting sensor data into quantitative feedback for material and printing process control, facilitating G-code management through an integrated interface. For such developments, our customized system provides problem-solving capabilities and iterative improvement features not found in commercial sensors. The contributions of this paper can be summarized as follows:

- This study presents a design method for a 2D laser profile sensing system for monitoring the extruded filament of the 3DCP process. By reducing design variables, the system meets the requirements of camera FOV, working distance, and installation space.
- The proposed 2D laser profile sensing system, integrated with a rotatable nozzle, enables quality monitoring of filament shape not only along linear paths but also along curved ones.
- Existing studies on geometric quality monitoring techniques provide only partial information on the extruded concrete filaments, such as width or height, and some studies are limited to linear paths.
- The proposed processing algorithm for a 2D laser profile sensing system can calculate not only width but also the height and cross-sectional area of the extruded concrete layer, enhancing geometric quality monitoring in the 3DCP process.
- This study presents a non-destructive, automated, inline quality assessment method, laying a crucial foundation for implementing an in-process quality control system for extrusion volume, nozzle stand-off distance, and material properties.

The rest of this paper is organized as follows: Section III describes the design of the 2D profile sensing system for 3DCP with the background of the modeling of the 2D profile sensing system. Section IV discusses the processing algorithm to compute the 2D profile data, including the width, thickness, and area of the extruded filament. Section V verifies the performance of the developed 2D laser profile sensing system through static and motion tests and its application in 3D concrete printing. Finally, Section VI summarizes the conclusions and future works. Furthermore, Appendices A and B provide additional information regarding the derivation of calibration parameters and the calibration experiment.

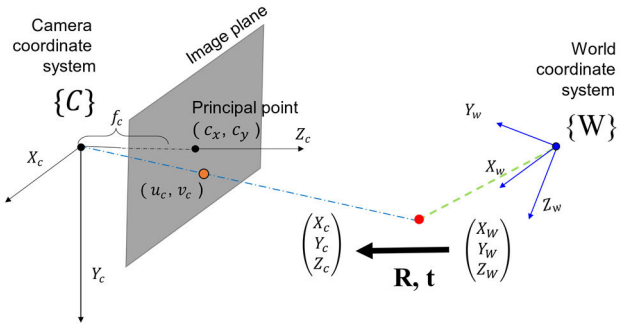

FIGURE 3. Perspective projection and coordinate transformation.

III. MODELING AND DESIGN OF 2D PROFILE SENSING SYSTEM FOR 3D CONCRETE PRINTING

A. MODELING OF 2D PROFILE SENSING SYSTEM

A 2D laser profile sensing system employs the laser triangulation principle which measures triangulated distance by projecting a laser beam at the target object and detecting the reflected light. By projecting a 2D laser beam onto the target and analyzing the projected laser line captured by the camera, the system can calculate the precise profile of the object. Laser triangulation offers notable advantages, including high accuracy and rapid data acquisition, making it well-suited for tasks that require precise and efficient measurements [25].

In this study, a 2D laser profile sensing system provides 2D profile data of the extruded concrete filament during 3D concrete printing. While the 2D line laser is projected on the filament, the camera captures the image, and the sensor evaluates the 2D profile data of the concrete filament. The pixel points of the image are transformed into world coordinates to assess the cross-sectional dimensions of the extruded concrete filament. Therefore, a coordinate transformation equation is required to map the image and world coordinates. This procedure can be made using each coordinate's relationships with the camera coordinate (see Fig. 3).

1) PERSPECTIVE PROJECTION

The relationship between 2D images and 3D space can be explained with perspective projection. For planar surface objects, any projective perspective transformation from 3D space to a 2D image can be modeled as a homography, as discussed later in this section. This study uses a method of converting world coordinates to camera coordinates and then projecting a point in camera coordinates into image coordinates. The world coordinate is located on the concrete filament, and the image coordinate is located on the camera's image sensor. A 2D point on the image plane is represented by $(u,\ v)$. The principal point, (c_x, c_y), is defined as the intersection point between the image plane and the Z-axis

of the camera coordinate system. The relationship between a 3D point in the camera coordinate system and its image projection is described as (1):

$$s\begin{bmatrix} u \\ v \\ 1 \end{bmatrix} = \begin{bmatrix} f_x & 0 & c_x & 0 \\ 0 & f_y & c_y & 0 \\ 0 & 0 & 1 & 0 \end{bmatrix} \begin{bmatrix} X_C \\ Y_C \\ Z_C \\ 1 \end{bmatrix} \tag{1}$$

When a camera is positioned within a 3D world coordinate system, a point $[X_w, Y_w, Z_w]$ represented in the world coordinate system can be expressed as $[X_c, Y_c, Z_c]$ in the camera coordinate system through coordinate transformation. This relationship involves a rotation matrix R and a translational vector $\boldsymbol{t}$ and can be expressed as (2).

$$\begin{bmatrix} X_c \\ Y_c \\ Z_c \\ 1 \end{bmatrix} = \begin{bmatrix} r_{11} & r_{12} & r_{13} & t_1 \\ r_{21} & r_{22} & r_{23} & t_2 \\ r_{31} & r_{32} & r_{33} & t_3 \\ 0 & 0 & 0 & 1 \end{bmatrix} \begin{bmatrix} X_w \\ Y_w \\ Z_w \\ 1 \end{bmatrix} \tag{2}$$

Here, the character r_{ij} represents the components of the rotation matrix R and t_i represents the components of the translation vector $\boldsymbol{t}$. In a 2D profile sensing system, when a 2D line laser is projected onto a plane with $Z_W = 0$, the laser points on the object can be represented as $[X_w Y_w 1]^T$, and the equation is then dimensionally reduced to the following form.

$$\begin{bmatrix} X_c \\ Y_c \\ Z_c \\ 1 \end{bmatrix} = \begin{bmatrix} r_{11} & r_{12} & t_1 \\ r_{21} & r_{22} & t_2 \\ r_{31} & r_{32} & t_3 \\ 0 & 0 & 1 \end{bmatrix} \begin{bmatrix} X_w \\ Y_w \\ 1 \end{bmatrix} \tag{3}$$

By combining (1) and (3), the homography equation is obtained, as expressed in (4):

$$s\begin{bmatrix} u \\ v \\ 1 \end{bmatrix} = \underbrace{\begin{bmatrix} f_x & 0 & c_x & 0 \\ 0 & f_y & c_y & 0 \\ 0 & 0 & 1 & 0 \end{bmatrix}}_{\text{Camera Intrinsic}} \underbrace{\begin{bmatrix} r_{11} & r_{12} & t_1 \\ r_{21} & r_{22} & t_2 \\ r_{31} & r_{32} & t_3 \\ 0 & 0 & 1 \end{bmatrix}}_{\text{Camera Extrinsic}} \begin{bmatrix} X_w \\ Y_w \\ 1 \end{bmatrix} \tag{4}$$

The homography equation consists of the extrinsic and intrinsic camera matrices, and they can be represented as the camera matrix C as follows:

$$s\begin{bmatrix} u \\ v \\ 1 \end{bmatrix} = \begin{bmatrix} C_{11} & C_{12} & C_{13} \\ C_{21} & C_{22} & C_{23} \\ C_{31} & C_{32} & C_{33} \end{bmatrix} \begin{bmatrix} X_W \\ Y_W \\ 1 \end{bmatrix} \tag{5}$$

2) MAPPING BETWEEN IMAGE PLANE AND WORLD COORDINATE

The camera's intrinsic and extrinsic parameters are used to reconstruct the three-dimensional information from the two-dimensional image [26]. From the previous section, the mapping equation from world coordinate to image coordinate was obtained by (5), and the C matrix comprises nine unknown parameters that are not fully independent. By dividing both sides of (5) by the constant C_{33}, it can be expressed as a simpler relationship, as given by (6):

$$s\begin{bmatrix} u \\ v \\ 1 \end{bmatrix} = \begin{bmatrix} h_{11} & h_{12} & h_{13} \\ h_{21} & h_{22} & h_{23} \\ h_{31} & h_{32} & 1 \end{bmatrix} \begin{bmatrix} X_W \\ Y_W \\ 1 \end{bmatrix} \tag{6}$$

This represents the transformation from the image coordinate to world coordinate, in which the equation includes eight unknown h_{ij}. Based on (6), a point in the world coordinate (X_i, Y_i) is mapped into a point in the image coordinate (u_i, v_i) by the following (7) and (8):

$$u_i = \frac{h_{11}X_i + h_{12}Y_i + h_{13}}{h_{31}X_i + h_{32}Y_i + 1} \tag{7}$$

$$v_i = \frac{h_{21}X_i + h_{22}Y_i + h_{23}}{h_{31}X_i + h_{32}Y_i + 1} \tag{8}$$

Conversely, a point (X_i, Y_i) in the world coordinate can be calculated from the given image pixel (u_i, v_i) as following:

$$\begin{bmatrix} X_i \\ Y_i \end{bmatrix} = \begin{bmatrix} u_i h_{31} - h_{11} & u_i h_{32} - h_{12} \\ v_i h_{31} - h_{21} & v_i h_{32} - h_{22} \end{bmatrix}^{-1} \begin{bmatrix} h_{13} - u_i \\ h_{23} - v_i \end{bmatrix} \tag{9}$$

The detailed derivation of (9) and calibration vector $\boldsymbol{h}$ is described in Appendix A [27].

B. DESIGN REQUIREMENTS

A customized low-cost 2D laser profile sensor is developed for in-situ geometry inspection of extruded concrete filament. The full view of the developed 2D laser profile sensor is shown in Fig. 4. Sensors used in 3DCP can be easily contaminated by dust, water, and fresh concrete. Therefore, it is not appropriate to use commercial 2D laser profile sensors costing at least $6,000 USD on a 3DCP construction site with high contamination risk. Securing cost-effective sensor technology is essential due to the frequent need for replacement and maintenance of sensor components caused by the risk of contamination from concrete. Moreover, the commercial sensors have bigger dimensions and measuring ranges than the dimension of the place to be installed, and therefore they cannot easily fit into the gap between the printed layer and the printing nozzle of the robotic arm 3D concrete printer. When the height of the sensor is increased, it is necessary to design the length of the upper connecting pipe of nozzle longer (Fig. 4(h)). However, this can result in increased vibrations during the horizontal movement of the robot arm. These vibrations can act as an interference to the accurate measurement of the 2D laser profile sensing system. The addition of heavy laser sensors would increase the print head weight and the inertia of the rotating part, leading to a cumbersome unit. Therefore, there is a clear need for compact, lightweight, and cost-effective customized sensors that can be applied in the field of 3DCP.

C. DESIGN OF 2D LASER PROFILE SENSING SYSTEM

Design of a 2D laser profile sensing system involves the choice of the camera's intrinsic and extrinsic parameters in (4), to meet the specified FOV criteria and the design

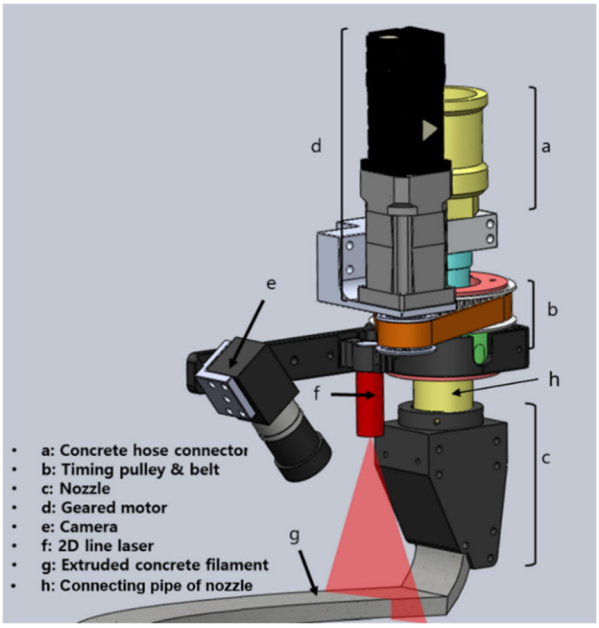

FIGURE 4. Schematic illustration of developed 2D laser profile sensing system for 3D concrete printing attached to the end of the rotatable nozzle.

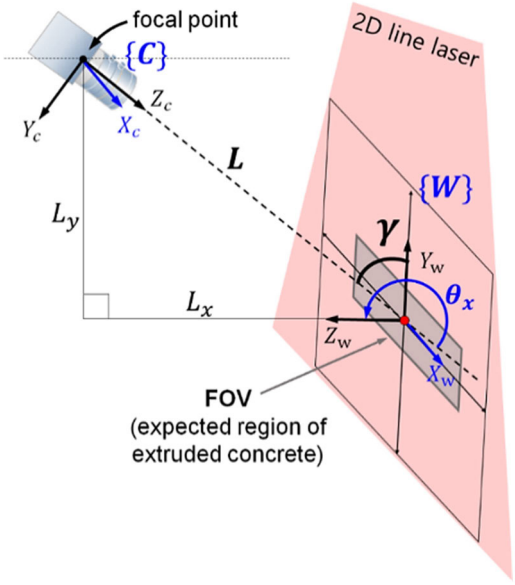

FIGURE 5. Calculating the expected mapping region using the laser triangulation method.

requirements. In other words, this process entails the careful selection of a camera and lens combination to map the FOV at the world coordinate plane to the camera's image coordinate plane. Additionally, it necessitates the determination of the camera's angle and position relative to the FOV plane, all while taking into account the aforementioned design requirements.

Considering the expected dimensions of concrete filament (44 mm in width and 11 mm in height), the FOV was chosen to have dimensions of 70 mm × 35 mm on the plane where the laser is projected.

1) SELECTION OF CAMERA AND LENS

The optical hardware of the sensing system consists of a 2D line laser and CMOS camera mounted with a lens and band-pass filter. Higher camera resolution results in better sensing accuracy; however, this leads to a decrease in frame rate and a proportional increase in processing time as the amount of data increases. As a suitable camera, Basler's acA1300-75gm model, a global shutter type with 8 mm focal length, was used in this study, which has a resolution of 1280 px × 1024 px and provides a maximum frame speed of 88 fps. The camera's CMOS sensor is a PYTHON 1300 with a pixel size of 4.8 μm × 4.8 μm (H × V). In addition, MOD should be as small as possible to satisfy the design requirement of the low-profile sensing system. Computar's M0814-MP2 F1.4 lens was selected with a MOD of 100 mm, compatible with a 2/3" type C-mount.

2) SELECTION OF DESIGN PARAMETERS

After selection of camera and lens, the camera angle (γ), the distance (L) from the camera's focal point to the origin of the FOV plane are determined by using a laser triangulation method to ensure that the FOV of the world coordinate plane can be mapped to the image coordinate plane of the selected camera system (See Fig. 5).

In (4), the focal length is set at 8 mm in accordance with the specifications of the selected lens, and the principal point on the image plane, (c_x, c_y), can be chosen as (640 px, 512 px) at the central position. Additionally, to match the units on both sides in (4), the focal length can be expressed as 8 mm / (4.8 μm/px), approximately equal to 1666.67 px, by considering the pixel size of the selected CMOS sensor. In Fig. 5, the orientation matrix ${}^{C}_{W}R$ represents the rotation of $\{W\}$ about the x-axis of $\{C\}$, and the translation vector ${}^{C}\boldsymbol{P}_{\boldsymbol{W\ org}}$ is the vector from the frame of $\{C\}$ to the origin of $\{W\}$. These rotation matrix and translation vector are expressed as follows:

$$R = {}^{C}_{W}R = \begin{bmatrix} 1 & 0 & 0 \\ 0 & cos\theta_x & -sin\theta_x \\ 0 & sin\theta_x & cos\theta_x \end{bmatrix} = \begin{bmatrix} r_{11} & r_{12} & r_{13} \\ r_{21} & r_{22} & r_{23} \\ r_{31} & r_{32} & r_{33} \end{bmatrix} \tag{10}$$

$$t = {}^{C}\boldsymbol{P}_{\boldsymbol{W\ org}} = \begin{bmatrix} \boldsymbol{0} \\ \boldsymbol{0} \\ \boldsymbol{L} \end{bmatrix} = \begin{bmatrix} \boldsymbol{t}_1 \\ \boldsymbol{t}_2 \\ \boldsymbol{t}_3 \end{bmatrix} \tag{11}$$

When γ represents the angle between the camera and the 2D line laser, and θ_x can be expressed as $270° - \gamma$.

It is worth noting that our sensor installation is subject to the height requirements imposed by the robot's arm profile, with L_y measuring approximately 109 mm. From the perspective of minimizing mechanical vibrations, having a longer L_y is not preferred, so L_y can be set to 109 mm. If the camera's position is maintained at a constant height, L_y, and its orientation is consistently adjusted to face the origin of $\{W\}$,

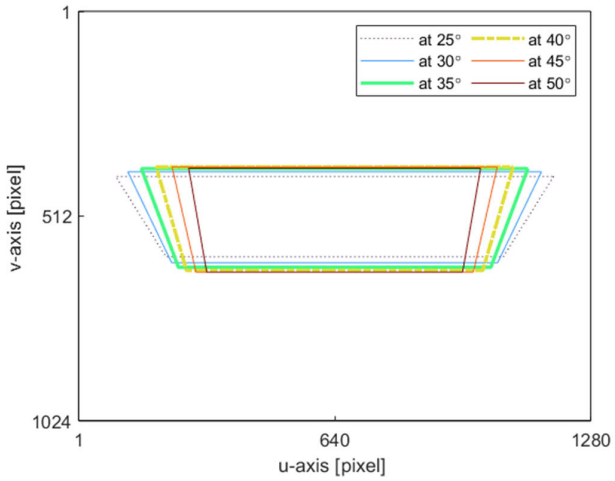

FIGURE 6. Projected target area on the image plane for various γ angles.

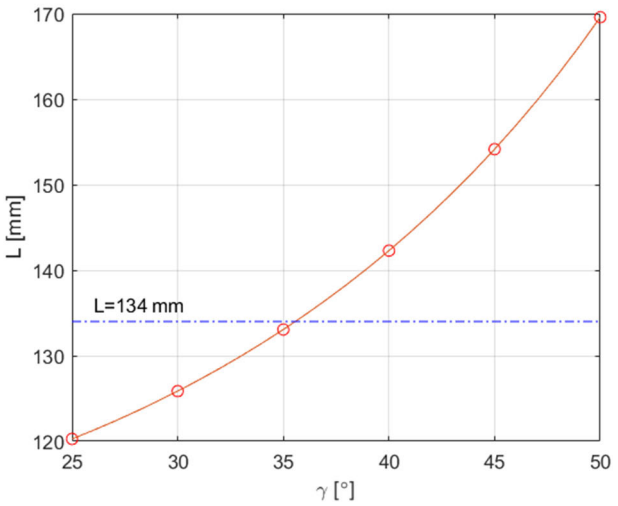

FIGURE 7. Relationship between γ angle and distance L from focal point to world coordinate origin.

the design problem of the 2D profile sensor can be simplified to a single design variable. Under such constraint conditions, once the design variable γ is determined, the distance L is automatically determined by $L_y/\cos(\gamma)$. Consequently, the relationship of a point (W_x, W_y, 0) on the 2D laser plane of $\{W\}$ being mapped onto the image plane can be expressed as a function of γ as follows:

$$s\begin{bmatrix} u \\ v \\ 1 \end{bmatrix} = \begin{bmatrix} 1666.7 & 0 & 640 & 0 \\ 0 & 1666.7 & 480 & 0 \\ 0 & 0 & 1 & 0 \end{bmatrix} \times \begin{bmatrix} 1 & 0 & 0 \\ 0 & \cos(270^\circ - \gamma) & 0 \\ 0 & \sin(270^\circ - \gamma) & L_y/cos\gamma \\ 0 & 0 & 1 \end{bmatrix} \begin{bmatrix} X_w \\ Y_w \\ 1 \end{bmatrix} \tag{12}$$

As γ varies from 25° to 50° in (12), the target area (70 mm × 35 mm) is mapped onto the image plane in various trapezoidal shapes, as shown in Fig. 6. Additionally, the relationship between γ and the distance L, from the camera's focal point to the origin of $\{W\}$ is shown in Fig. 6. As the camera angle γ increases from 25° to 50°, the distance L from the camera's focal point to the origin of {W} varies from approximately 120 mm to 170 mm. In Fig. 6, it can be observed that when γ is small, the projected target area (trapezoidal shape) on the image plane occupies a wide range within the full 1280 pixel area. As γ increases, the proportion of the trapezoidal width decreases, leading to a relative disadvantage in terms of sensing resolution. This occurs due to the increasing distance between the camera and the object. Additionally, a larger γ results in an increased L_x, which is not preferred in terms of the sensor's compactness requirement. In summary, from the perspectives of sensing resolution and compactness, a smaller γ is preferable.

Furthermore, considering the distance of approximately 34 mm from the focal point to the front surface of the selected lens (lo), and the MOD requirement of 100 mm between the front surface of the lens and the object, the minimum value of the distance L from the focal point to the object becomes approximately 134 mm. According to the relationship shown in Fig. 7, this implies that the gamma angle should be chosen to have at least 36°. Consequently, the design variable gamma was chosen as 37°, corresponding to an L value of 136.5 mm.

D. INTEGRATION WITH A ROTATABLE NOZZLE

The developed sensor was attached to a rotatable nozzle of a robotic arm 3D concrete printer to ensure measurement at both linear and curved printing paths as shown in Fig. 4. The rotatable nozzle comprises a concrete hose connection, geared motor, pulley, belt, and nozzle. It has a rotation speed of 60 rpm with a maximum rotation speed of 120 rpm, and it can rotate infinitely, exceeding 360 degrees. The extruding part of the nozzle is rectangular shaped and has dimensions of 44 mm ×10 mm (width × thickness). The 2D laser profile sensor is attached to the rotatable part to detect the surface of the deposited concrete layer following the printing path, including straight and curved paths. Without the rotatable nozzle, the sensor can only detect the profile of the concrete filament extruded in a straight line in a specific direction. It cannot detect the profile when the nozzle moves along an arbitrary printing path in the printing workspace. A sensing system with multiple sensors might be an alternative, but it requires additional costs.

Given the stiff printing material's ability to retain its shape due to its intrinsic high yield stress, the distance between the laser source and the nozzle center was considered non-critical for this study. Nevertheless, for printing materials with high viscosity, it's advisable to conduct preliminary tests to ascertain the time required for the material to transition from a transient to a steady state. This prior assessment should guide the adjustment of the laser-nozzle center distance and the printing speed accordingly.

IV. PROCESSING ALGORITHM TO COMPUTE THE PROFILE INFORMATION OF EXTRUDED CONCRETE FILAMENT

The real-time 2D profile detection system was designed to collect the height, width, cross-sectional area, and extrusion rate of the extruded concrete filament by acquiring and processing the image. A flowchart of image processing of the 2D laser profile sensing system is shown in Fig. 8. First, the camera captures the image of the laser-projected concrete filament. The image is originally 1280×1024 pixels, but we sampled 1280×545 pixels for faster processing by limiting the region of interest (ROI) to the area under the nozzle. The camera used in this image is monochrome since it has higher sensitivity, higher resolutions, and better performance in low-lighting conditions [28]. Then, the image segmentation is made to subtract the pixel point cloud representing the laser line with the thresholding method. The position of the laser line is then defined using the center of gravity method. The defined laser line is then divided into upper and bottom parts, representing the layer surface and the ground, respectively. For example, k-nearest clustering method can be used [29]. Each pixel data set in the image coordinate is then transformed into the world coordinate using the transformation matrix (10). The reference ground line is defined using a first-order linear regression based on the data points on bottom parts. Finally, 2D profile data, including cross-sectional area, thickness, and width, are calculated using the pixel coordinate values of the upper part, bottom part, and reference ground line. Detailed explanations will be provided in the following paragraph.

A. IMAGE SEGMENTATION: THRESHOLDING

As the image of the laser line on the extruded concrete layer is collected (as shown in Fig. 9(a)), the Otsu algorithm is applied to automatically determine an optimal threshold for image segmentation, based on the intensity distribution of pixel values [30]. If pixel values lower than the Otsu threshold intensity are converted to zero intensity values, the pixels in the image are then separated into two groups: perfect background and laser light pixels. Although the detected laser point is a white color pixel with high intensity, for convenience in visualization, the laser point cloud is represented in black from Fig. 9(b) to Fig. 9(i).

B. EXTRACTION OF LASER PROFILE USING CENTER OF GRAVITY METHOD

In Fig. 9(b), the image after image segmentation can include multiple laser points along a vertical axis. So the data for accurate laser profile should be determined. Fig. 9(k) shows the extraction of the profile using the center of gravity method [31]. The position of the line laser pixel is denoted by p_i and the intensity value of p_i is represented as $I(p_i)$. By employing the center of gravity method using (13), the 2D laser profile of the layer cross-section is calculated in a sub-millimeter unit. The collection of the determined laser line along the vertical axis is presented in Fig. 9(c).

$$P_{cog}(i) = \frac{\sum_{j=1}^{N} I(p_j) \cdot p_j}{\sum_{j=1}^{N} I(p_j)}$$
$$\text{if } I(p_j) < \text{threshold}, \quad I(p_j) = 0 \tag{13}$$

C. SEPARATION OF LASER PROFILE USING CLUSTERING METHOD

The defined laser line can be separated into the upper and bottom parts using the k-nearest clustering method (KNN) [29], as shown in Fig. 9(d). However, the KNN method requires considerable processing time, and therefore the laser line is classified by using the threshold, which is determined by the average value of detected points of the laser profile. The average position of $P_{cog}(i)$ is used as a threshold to divide the 2D profile laser line into the upper part and bottom part (Fig. 9(e)). Here, the upper part represents the top surface of the extruded filament, and the bottom part represents the ground. The pixel points of the defined laser line are separated into P_{up} if the position is lower than P_{avg}, and P_{bot} if the position is higher than P_{avg}.

D. COORDINATE TRANSFORMATION FROM {C} TO {W}

The defined laser position (u_i, v_i) is converted to the points in the world coordinate (X_i, Y_i) using (9). The corresponding world coordinates in the upper part are $(P_{up_{x_i}}, P_{up_{y_i}})$, and in the bottom part are $(P_{bot_{x_i}}, P_{bot_{y_i}})$, respectively.

E. ESTIMATION OF REFERENCE GROUND LINE BY LINEAR REGRESSION

As the laser line is separated into the upper and bottom lines, the bottom line is defined using the first-order linear regression [32] as a function $y = f_{bot}(x)$ from the data of $(P_{bot_{x_i}}, P_{bot_{y_i}})$. From this best-fitting line, the estimated ground points below the upper profile points are calculated. The resulting ground line is depicted as a green line, as shown in Fig. 9(f).

F. CALCULATION OF THE PROFILE INFORMATION (CROSS-SECTIONAL AREA, AVERAGE THICKNESS, MAXIMUM WIDTH)

In this section, the cross-sectional area, average thickness, and maximum width of the extruded concrete filament are calculated. The cross-sectional area is estimated by numerical integration of the thickness and width values of infinitesimal elements, as shown in Fig. 9(g). The area of the printed concrete layer, denoted as $A_{cross-section}$, is then estimated using the trapezoid rule as follows:

$$A_{cross-section} = \sum_{i=0}^{m-2} (x_{i+1} - x_i) \frac{h(x_i) + h(x_{i+1})}{2} \tag{14}$$

The extrusion rate is calculated by multiplying the cross-sectional area by the extrusion velocity,

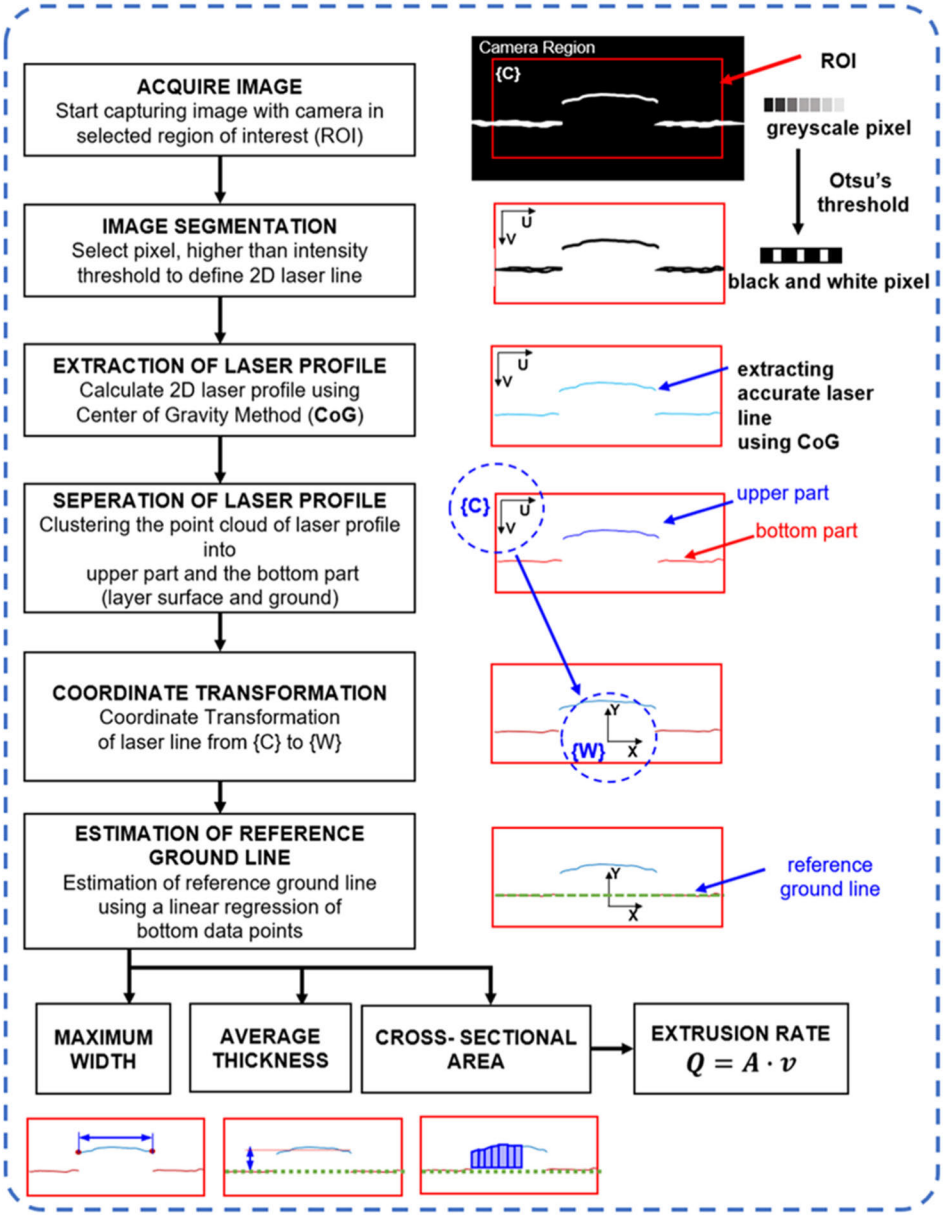

FIGURE 8. Flow chart of processing algorithm for calculating profile information of extruded concrete.

as shown in (15).

$$Q_{measured} = A_{cross-section} \cdot v \tag{15}$$

The average thickness is determined by calculating the mean gap between the upper part and the estimated bottom part, which is expressed as (16), where m represents number of pixels for P_{up}. The procedure for calculating the thickness is illustrated in Fig. 9(h).

$$\begin{aligned} t_{thickness} &= \sum_{i=0}^{m-1} \frac{P_{up_{x_i}} - \hat{P}_{bot_{x_i}}}{m} \\ &= \sum_{i=0}^{m-1} \frac{P_{up_{x_i}} - f_{bot}\,(x_i)}{m} \end{aligned} \tag{16}$$

The width of the extruded concrete filament is calculated by subtracting the minimum value of $P_{up_{x_{min}}}$ from the maximum value of $P_{up_{x_{max}}}$, as shown in (17). Fig. 9(i) shows how the width of the upper profile is calculated. Here, $P_{up_{x_{min}}}$, $P_{up_{xmax}}$ represent the minimum and maximum positions of $P_{up_{x_i}}$, respectively.

$$w_{width} = P_{up_{x_{max}}} - P_{up_{x_{min}}} \tag{17}$$

G. OUTPUT OF 2D PROFILE SENSING SYSTEM

When operating the 2D profile detection system, 2D laser line profile position data are transformed into world coordinate values. These are then displayed using OpenCV during the operation, as shown in Fig. 9(j). In this display, the detected

2D profile points, comprising the upper and ground parts are shown in red, while the blue line represents the estimated bottom part below the upper profile. Simultaneously, data on the cross-sectional area, average thickness, and width value are collected and transmitted to the main PC.

H. DATA TRANSMISSION

The data transmission mechanism is described in the flow chart shown in Fig. 10. In this study, G-code included X, Y, and Z positions, printing speed F, the rotation angle R of the rotatable nozzle, and extrusion information E. As G-code is imported to the main controller, reference position commands are transmitted to each servo motor. There is a total of six servo motors. The robotic arm 3D printer has four motors that allow 4 DOF motion. Since EtherCAT communication is adopted between the main controller and the servo controller, additional axes, such as the rotatable nozzle and extruder, can be added and fully synchronized with the motion of the robotic arm.

During 3D concrete printing, a 2D profile detection system based on a mini-PC collects the 2D profile data. It can also be controlled by a laptop connected through a local wireless network. The 2D profile data (area, width, and height) are transmitted to the main controller using 16-bit format through Controller Area Network (CAN) communication.

V. EXPERIMENTAL VALIDATION OF THE 2D LASER PROFILE SENSING SYSTEM

This section presents the experimental results of the proposed 2D laser profile sensing system under various conditions, including static, motion, and concrete 3D printing tests. Through these three experiments, which vary in terms of ground plane conditions (flatness), scanned objects, and transport conditions including vibration sources, it is possible to closely examine the reasons and characteristics of errors that occur when applying the 2D laser profile system to 3D concrete printing. The fundamental accuracy of the system is verified through static and motion tests on a target of known size. Then, a comprehensive assessment is conducted on the profile measurement results of the extruded concrete filaments during the printing process.

A. PERFORMANCE OF DEVELOPED 2D PROFILE DETECTION SYSTEM UNDER STATIC CONDITION

1) EXPERIMENTAL SETUP FOR STATIC TEST

In this section, two-axis linear stages are used to accurately evaluate the performance of 2D laser profile sensing systems under static conditions, as shown in Fig. 11. The experiment is performed to validate the sensor's accuracy in every position of the FOV. Therefore, to ensure accurate area data are obtained from every possible position in the FOV of the camera, 2D profile data of a plastic block of known size were collected from nine different positions. The calculated data, including width, thickness, and area, were acquired while moving the position of the 2D profile detection sensor using

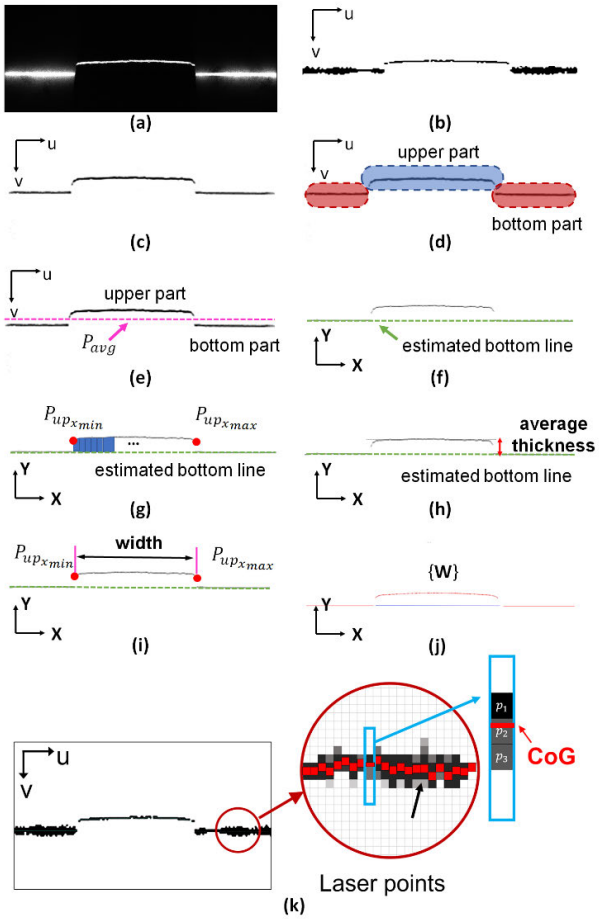

FIGURE 9. Procedure for calculating the 2D profile. (a) Acquired image. (b) Segmented laser point cloud generated using Otsu's algorithm. (c) Defined laser line. (d) Clustered laser line into the upper part and bottom part, (e) Laser separation by average laser position, P_{avg}. (f) Estimated reference ground line using 1st order linear regression. (g) Calculating the area of the 2D cross-sectional profile. (h) Calculating the average thickness. (i) Calculating the maximum width of the upper profile. (j) Visualized 2D laser profile in world coordinate. (k) The laser line is defined using the center of gravity method.

2-axis linear stages with a motion controller. The linear stage allows a travel range of 200 mm, which can cover the movement range of the nozzle head during 3D concrete printing and has an accurate resolution of 0.1 μm. Additionally, the block with a cross-section size of 40 mm $\times$ 10 mm (width $\times$ thickness) was used for the static test, which simulated the dimensions of the nozzle and the extruded concrete layer.

2) ACCURACY ANALYSIS FOR TEST UNDER STATIC CONDITION

The 2D profile data of the block were collected from nine different positions under static conditions, and their accuracy was analyzed. The 2D profile sensing system was shifted to nine positions, varying by $\pm$10 mm in both horizontal and vertical directions, as shown in Fig. 11. Here, Y_0 represents the default stand-off distance between the camera and the center of FOV. P1 denotes a point Y_0 down from the camera position, and P2 denotes the center position of the top of the

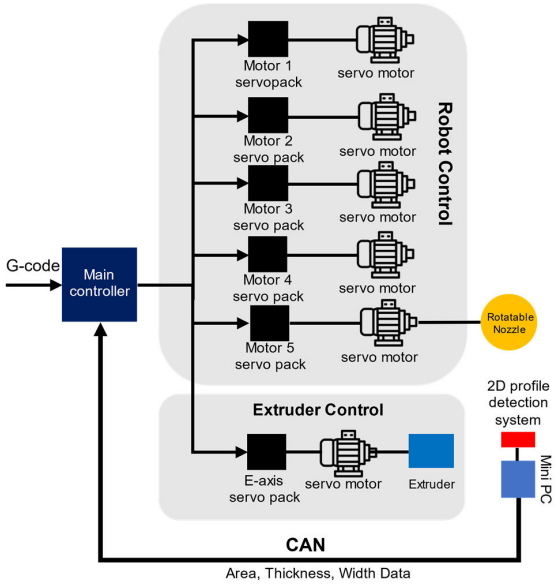

FIGURE 10. Overall control system of the in-situ quality monitoring for 3D concrete printing.

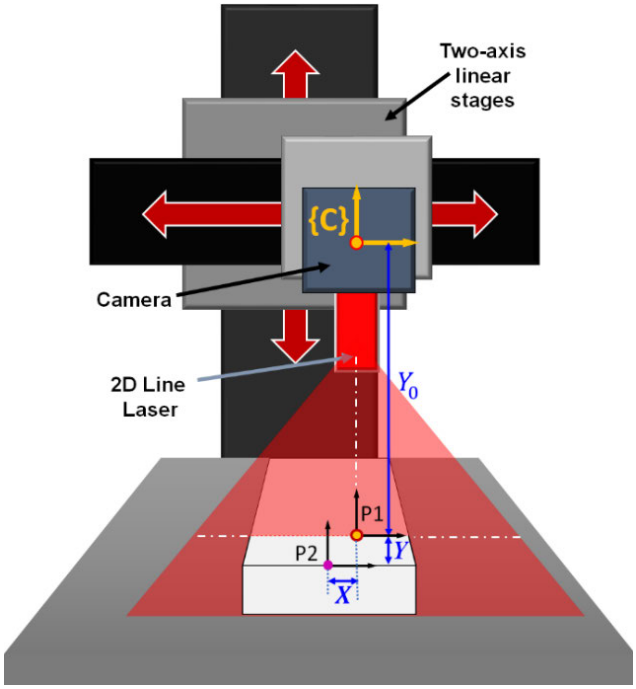

FIGURE 11. Experimental setup for a static test. Two-axis linear stages were used to change the position of the 2D laser profile detection sensor. The beam of a 2D line laser is projected on the block.

block. The relative position of P1 with respect to P2 is denoted by (X, Y). During the static test, the 2D line laser is projected onto the block, and the camera acquires its image. The image data are then processed to world coordinate data using (10) and visualized during the test, as shown in Fig. 12. The red line in the image represents the ground and object surface, the blue line represents the estimated bottom of the object calculated from the regression line of the detected ground profile, and the cross-section area of the object was calculated with the method described in Section IV.

The measurement results during the static test are shown in Table 3. The measured average values for width and thickness were very precise, closely aligning with the actual values of 40 mm and 10 mm, with measured averages of 39.99 mm and 10.07 mm, respectively. Additionally, the measured area exhibited a high level of precision, with an average value of 402.50 mm^2, representing a relative error of only 0.625% compared to the actual area of 400 mm^2. This experiment under static condition shows the best precision among the three experiments because measurements are conducted on a single object with almost no external vibration. The two-axis stage ensures pure translational motion, and its base machined from metal exhibits perfect flatness compared to other experimental conditions.

B. PERFORMANCE TEST OF 2D PROFILE DETECTION SYSTEM DURING MOTION

1) EXPERIMENTAL SETUP FOR TEST DURING MOTION

In this section, the measurement accuracy of the developed sensing system was verified while operating the robot by attaching the sensing system to the end effector. The results of the width, thickness, and cross-sectional area measurements were examined.

The robotic arm 3D concrete printer developed at the Construction Robot and Automation Laboratory of Yonsei University was used for this test. The current version of the robot arm basically has four degrees of freedom (DOF), including one yawing axis and three pitching axes, and it can locate the end effector in 3D space with an additional degree of freedom of pitch angle at the end effector. A rotatable printing nozzle is attached to the end effector of the robotic arm 3D printer, as shown in Fig. 13(a). The robot arm can reach up to two meters in a cylindrical workspace. Additional servo motors on the material extruder and rotatable nozzle are connected to the main controller of the robotic arm 3D printer for concrete pumping to the print head. Fig. 13(b) illustrates the scanning of the 2D profile of connected rectangular plywood bars, performed by moving the sensing system attached to the end effector at a speed of 20 mm/sec.

2) ACCURACY ANALYSIS FOR TEST DURING MOTION

The measurement results of the test during motion were plotted together with the ideal value (colored line) in Fig. 14. The measurement results of the width, thickness, and area of the plywood bar using the developed sensor during motion are summarized in Table 4. The measured values were compared with the true values of 50 mm width and 12 mm height, which are the cross-sectional dimensions of the plywood bar. The Mean Absolute Errors (MAEs) for the calculated width, thickness, and area are 0.56 mm, 0.21 mm, and 10.42 mm^2, respectively. The corresponding normalized MAEs are 1.12%, 1.75%, and 1.73%, respectively, signifying the errors as a percentage of the true values. Here, scanning

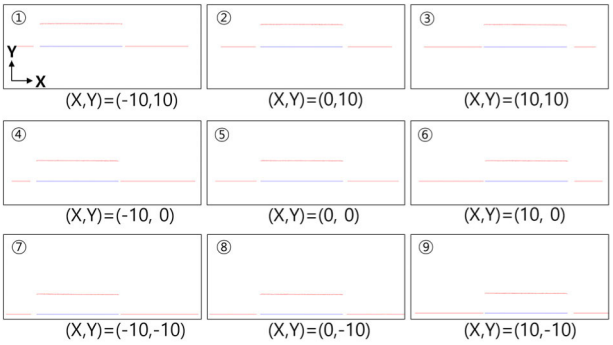

FIGURE 12. Acquired image data are processed and visualized during the static test. 2D profile data are collected from nine different positions within the range of FOV. The upper red line, bottom red line, and bottom blue line represent the object surface, ground, and bottom of the object, respectively.

TABLE 3. Statistical analysis of 2D profile measurement under static conditions. Block dimensions: 40 mm × 10 mm (width × thickness).

	Average value	Average error	Mean absolute error	Standard deviation
Width (mm)	39.99	-0.01	0.05	0.08
Thickness (mm)	10.07	0.07	0.07	0.05
Area (mm^2)	402.50	2.50	2.58	2.30

was conducted on a pallet made of plastic, which is the same floor condition as the 3DCP experiment, and provides flatness conditions less precise than those in static experiments. Increasing errors compared to static experiments are not only due to the flatness of the floor but also attributed to the motion generated by the robotic arm, which includes the cause of vibrations. Nevertheless, test results during motion demonstrate that the mean absolute error for both width and thickness is sufficiently accurate to be applicable to the operation of 3D concrete printing.

C. IN-SITU TESTING OF 2D PROFILE DETECTION SYSTEM DURING 3D CONCRETE PRINTING

1) EXPERIMENT USING A CONCRETE EXTRUDER AND ROBOTIC ARM 3D PRINTER

The 2D profile data were obtained in real-time using the developed system while extruding the concrete layers on the printed bed (Fig. 15). The processed 2D profile image of the extruded concrete layer was visualized in real-time with OpenCV, as shown in Fig. 16, where the red lines on the left and right side represent the ground, and the red line at the center represents the surface of the concrete layer. The printing speed was kept constant at 20 mm/sec, and the total length of the printed structure was 2656.6 mm. The final printed concrete layer is shown in Fig. 17.

2) DATA ANALYSIS OF 2D PROFILE SENSING SYSTEM DURING 3D CONCRETE PRINTING

The real-time measurement results for the width, thickness, and area, along with their average values (represented by the dotted line), for the printed concrete filament are shown

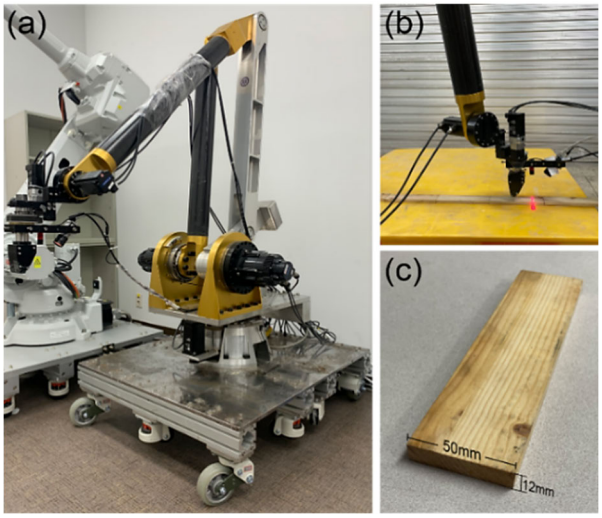

FIGURE 13. Experimental setup for test during motion. (a) robotic arm 3D printer of Yonsei University. (b) performance test during motion. (c) dimensions of plywood.

TABLE 4. Statistical analysis of 2D profile measurement during motion. Plywood bar dimensions: 50 mm × 12 mm (width × thickness).

	Average value	Average error	Mean absolute error	Standard deviation
Width (mm)	49.44	-0.56	0.56	0.14
Thickness (mm)	12.20	0.20	0.21	0.13
Area (mm^2)	590.18	-9.82	10.42	7.30

in Fig. 18. To calculate the error, the true values of width and thickness were obtained using a vernier caliper at several locations and are indicated by colored circles on the plot. Additionally, the true value of the area was calculated as the product of the width and thickness obtained from the vernier caliper. The statistical results of 2D profile measurement are shown in Table 5. The calculated width, thickness, and cross-sectional area for the extruded concrete filament showed MAE values of 1.22 mm, 0.72 mm, and 22.79 mm^2, respectively. When compared to the experimental results on the plywood bar during motion, the error increased approximately 2 to 3 times. The standard deviation of these measurements also increased compared to the previous values.

This is attributed to the characteristics of the extruded concrete filament material and the vibrations introduced by concrete pumping through the concrete hose. Normalized MAEs (MAEs relative to the vernier caliper measurements) on width, thickness and area are 2.79%, 6.65%, and 4.70%, respectively. When the averages of scan measurement are used as reference values instead of the vernier caliper values, the corresponding normalized MAEs are 1.10%, 3.72%, and 3.58%, respectively. Compared to the test results during motion (1.12%, 1.75%, and 1.73%, respectively), the performance for width is almost identical, but the relative error

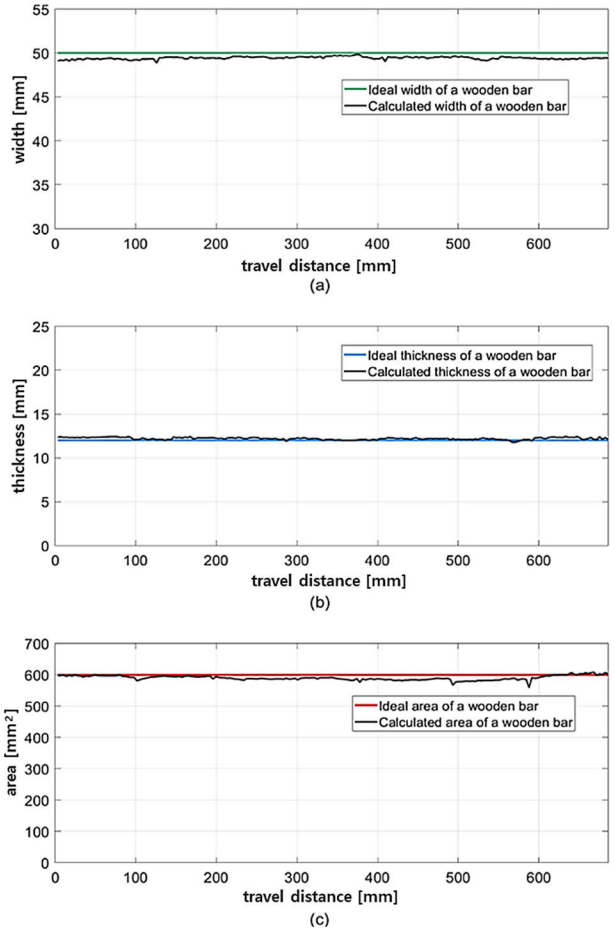

FIGURE 14. Calculated profile information of the plywood bar during the motion. (a) width. (b) thickness. (c) cross-sectional area.

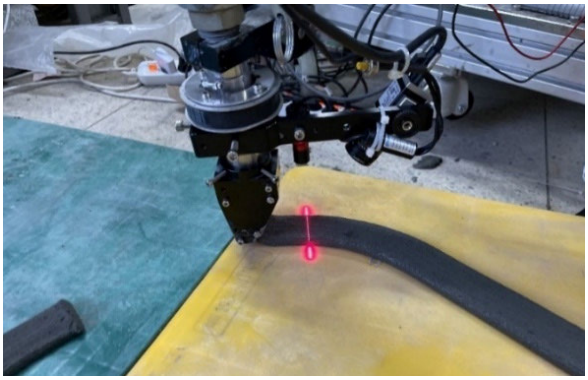

FIGURE 15. In-situ testing of 2D profile detection system during 3D concrete printing. The developed sensor acquires the 2D profile data of extruded concrete filament along curved printing path.

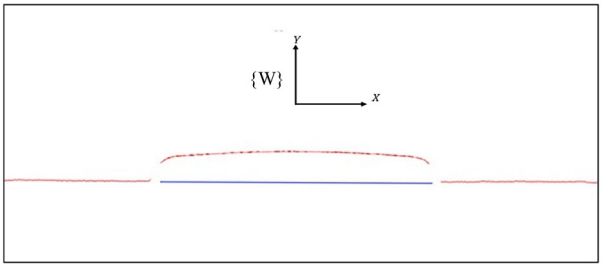

FIGURE 16. Processed 2D profile of extruded concrete filament during 3D concrete printing.

FIGURE 17. Final printing path of the experiment.

TABLE 5. Statistical analysis of 2D profile measurement for the extruded concrete layer during 3D concrete printing. In this table, true values refer to the measurements obtained using a vernier caliper.

	Average value	Average error	Mean absolute error	Standard deviation
Width (mm)	42.66	-1.11	1.22	0.68
Thickness (mm)	10.71	-0.11	0.72	0.76
Area (mm^2)	473.15	-11.66	22.79	18.21

for thickness and cross-sectional area has roughly doubled. The high variations in the measured thickness of filament can be attributed to voids and tearing in the printed filament, which are printing material and printing process-induced flaws [5]. The variation in the measured cross-sectional area and thickness of printed concrete represent that the developed monitoring system has sensed these flaws in the printed filament. Extruded concrete filaments, characterized by a low water-cement ratio, often exhibit a non-smooth surface, which frequently leads to defects such as voids and tearing in the printed concrete. These irregularities can contribute to variations in concrete thickness, thereby resulting in a relatively larger MAE in thickness.

In summary, the calculated MAE for thickness and width of 0.72 mm and 1.22 mm, respectively, can be regarded as having sufficient accuracy considering the maximum aggregate size of 1 mm in the concrete mixture used. The experimental results during 3D concrete printing show the suitability and accuracy of the developed sensing system to compute the shape information and demonstrate the developed system's feasibility for in-situ quality monitoring during the 3DCP process. The cross-section of the extruded concrete obtained during the 3DCP experiment may not be a perfect rectangular shape, as depicted in Fig. 16. The higher the yield stress of the material, the better the shape stability, which makes the extruded filament closer to the nozzle's rectangular shape. Conversely, as the yield stress decreases, material flowability improves, allowing the material to spread more widely without a distinct edge shape on the top corners of the cross-section [33], [34]. The results from the experiment,

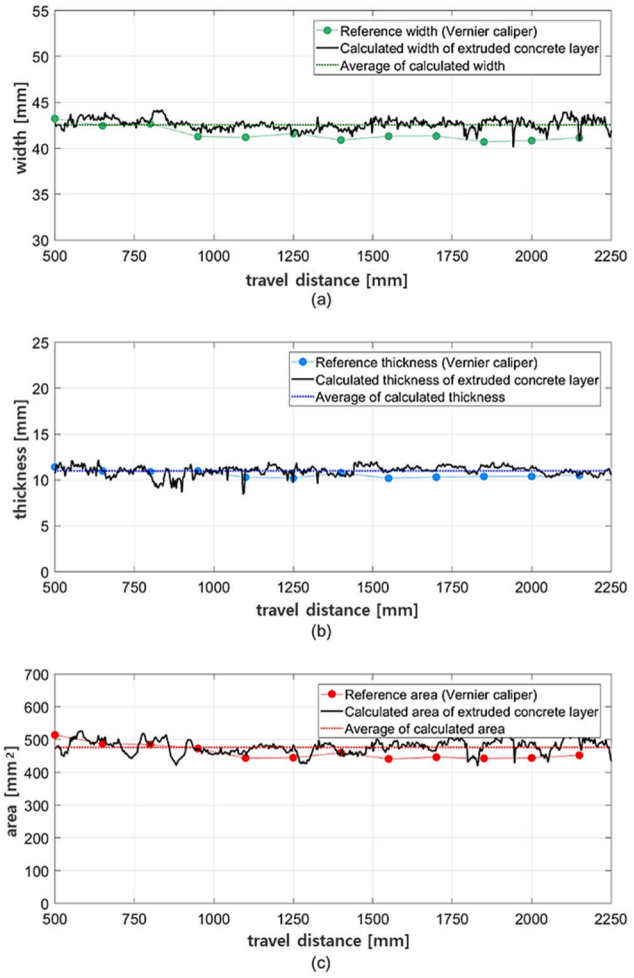

FIGURE 18. Calculated profile information of the extruded concrete filament during 3D concrete printing. (a) width. (b) thickness. (c) cross-sectional area.

as shown in Fig. 18, demonstrates that the current 2D profile sensing system can accurately acquire this cross-sectional shape information, which can be valuable for future research relating the cross-sectional shape information with material properties.

VI. CONCLUSION AND FUTURE WORKS

A comprehensive overview of the development of a 2D laser profile sensing system tailored for real-time geometric quality monitoring of extruded concrete in 3DCP is presented in this paper. The main conclusions of this study in terms of design, algorithm, and system are as follows:

A. DESIGN OF THE 2D LASER PROFILE

In this study, a systematic procedure was presented for determining design variables that meet the FOV, MOD, physical dimensions, and the specific requirements of 3DCP in the design of the 2D laser profile sensing system. The primary advantage of the proposed design method lies in its simplicity, and once the combination of camera and lens is selected, the design problem is converted into a problem of solving a single design variable based on the constraint on the height limit of the sensor. The proposed design method helps facilitate the design of a 2D laser profile sensing system by easily deriving design variables to suit the requirements of the 3DCP system being used. In addition, by integrating the developed sensing system into a nozzle device capable of infinite rotation, its usability has been enhanced to enable cross-sectional measurement of the concrete filament extruded in all directions along the printing path. This was demonstrated in the 3DCP printing experiment, which included both curved and straight segments of the 3D printing path, providing continuous monitoring information. Since this sensing system can be configured on a component basis, it can easily address contamination on the front camera lens by replacing the mounted protective filter. Additionally, it offers the possibility of adjusting the intensity of the 2D line laser based on ambient lighting conditions, unlike commercial products. While it's worth noting that this developed system has not been evaluated under outdoor printing conditions, these customization and flexibility advantages stand out in comparison to existing off-the-shelf sensors.

B. PROCESSING ALGORITHM FOR CROSS-SECTIONAL INFORMATION

The proposed processing algorithm to compute the profile information of the extruded filament involves stages of image segmentation, extraction, and clustering for the laser profile, followed by coordinate transformation, estimation of the reference ground line, and calculation of the profile, width, thickness, and area of the filament cross-section. Through the calibration process and experiments presented in the Appendix, the sensing system was calibrated to a MAE accuracy of 0.087 mm across the designed FOV area. To ascertain the feasibility of the sensing system, experiments were conducted on an industrial-scale robotic arm. The MAE values for the width and thickness calculated for the concrete filament during printing were 0.72 mm and 1.22 mm, respectively, which are very accurate values considering the maximum size of the concrete aggregate used, and the MAE value for the cross-sectional area was 22.79 mm^2. This experimentally verifies that the proposed processing algorithm effectively captures important information about extruded concrete filaments, including width, thickness, and cross-sectional area. The cross-sectional dimensions and the profile shape of the extruded concrete layer recorded in the system are valuable data points for proof of print quality and subsequent applications. This data can also be used to compute the concrete extrusion rate by multiplying the cross-sectional area by the nozzle travel speed.

C. SENSING SYSTEM

A stand-alone embedded PC-based sensing system interfaces with the sensing unit, consisting of a camera, lens, and 2D line laser, to acquire image information. It processes the

image in real-time using the proposed algorithm and transmits the resulting cross-sectional information to the main control unit through communication. The current embedded system used in the experiment calculated the width, thickness, and cross-sectional area and transmitted the data at approximately 4 Hz. To utilize the results of quality monitoring more effectively, it is necessary to update the calculated information more quickly. This requires high-performance hardware configuration and software optimization.

The application scope of the system developed and experimentally validated in this study was focused on monitoring the geometric print quality, specifically by assessing the dimensional accuracy of extruded concrete layers through profile detection. Looking forward, it is essential to develop technologies that not only measure geometrical information but also provide comprehensive quality information during the printing process. For instance, expanding this research to include predictions of material properties based on geometrical data could be highly beneficial. By investigating the relationship between material properties and the scanned profiles of extruded layers, a more holistic monitoring of concrete quality can be achieved, taking into account both geometric and material factors. Additionally, exploring the application of deep learning-based computational methods for analyzing extruded concrete filament shapes presents an intriguing opportunity.

The integration of the 2D profile sensing system into a closed-loop quality control framework not only enables real-time adjustments during printing but also acts as a springboard for further innovations in the field. Given the inherent characteristics of 3DCP, wherein the printing quality is easily influenced by the variability of materials used, the ability to measure the dimensions of extruded concrete in real time is crucial for improving the reliability and efficiency of 3D concrete printing processes. This comprehensive approach to quality control, potentially augmented with advanced material assessment and deep learning techniques, contributes to the ongoing evolution and enhancement of 3DP technology in the construction industry.

In conclusion, the developed 2D profile sensing system offers a robust solution for real-time geometric quality monitoring in 3D-printed concrete layers, representing a significant step towards enhanced print quality assurance in the 3DCP construction sector.

APPENDIX A
DERIVATION OF CALIBRATION PARAMETERS AND TRANSFORMATION FROM IMAGE TO WORLD COORDINATE

In this section, an effective yet straightforward calibration method suitable for use with 2D laser profiles is presented. The unknown calibration parameters, h_{ij}, can be determined from n-pairs of datasets regarding the point (u_i, v_i) in the image coordinate and the point (X_i, Y_i) in world coordinate. Rearranging the calibration matrix h of (6) into vector form gives the following (18).

$$\underbrace{\begin{bmatrix} X_1 & Y_1 & 1 & 0 & 0 & 0 & -u_1X_1 & -u_1Y_1 \\ 0 & 0 & 0 & X_1 & Y_1 & 1 & -v_1X_1 & -v_1Y_1 \\ X_2 & Y_2 & 1 & 0 & 0 & 0 & -u_2X_2 & -u_2Y_2 \\ 0 & 0 & 0 & X_2 & Y_2 & 1 & -v_2X_2 & -v_2Y_2 \\ & & & & \vdots & & & \\ X_n & Y_n & 1 & 0 & 0 & 0 & -u_nX_n & -u_nY_n \\ 0 & 0 & 0 & X_n & Y_n & 1 & -v_nX_n & -v_nY_n \end{bmatrix}}_{\boldsymbol{A}_{(2n\times 8)}} \underbrace{\begin{bmatrix} h_{11} \\ h_{12} \\ h_{13} \\ h_{21} \\ h_{22} \\ h_{23} \\ h_{31} \\ h_{32} \end{bmatrix}}_{\boldsymbol{h}_{(8\times 1)}} = \underbrace{\begin{bmatrix} u_1 \\ v_1 \\ u_2 \\ v_2 \\ \vdots \\ u_n \\ v_n \end{bmatrix}}_{\boldsymbol{b}_{(2n\times 1)}} \tag{18}$$

To solve the eight unknown elements in vector $\boldsymbol{h}$ of (18), at least four pairs of image and world coordinate datasets are necessary. In cases where more than four pairs of datasets are used, making A, a non-square matrix, the solution for calibration vector $\boldsymbol{h}$ can be determined using the pseudo inverse, which produces the minimum possible error in a least squares sense as shown in (19).

$$h = (A^T \cdot A)^{-1} A^T b \tag{19}$$

Now, using (7) and (8) with the h parameters obtained from (19), it is possible to calculate the corresponding image coordinate from the given world coordinate data. Conversely, the transformation equation from the measured camera image to the world coordinate can also be derived. Expressing X_i and Y_i as u_i and v_i in (7) and (8) gives (20). By multiplying the inverse matrix to both sides of (20), we can calculate the actual point (X_i, Y_i) in world coordinate from the image pixel (u_i, v_i), using h parameters obtained from (19), as depicted in (21).

$$\begin{bmatrix} u_ih_{31} - h_{11} & u_ih_{32} - h_{12} \\ v_ih_{31} - h_{21} & v_ih_{32} - h_{22} \end{bmatrix} \begin{bmatrix} X_i \\ Y_i \end{bmatrix} = \begin{bmatrix} h_{13} - u_i \\ h_{23} - v_i \end{bmatrix} \tag{20}$$

$$\begin{bmatrix} X_i \\ Y_i \end{bmatrix} = \begin{bmatrix} u_ih_{31} - h_{11} & u_ih_{32} - h_{12} \\ v_ih_{31} - h_{21} & v_ih_{32} - h_{22} \end{bmatrix}^{-1} \begin{bmatrix} h_{13} - u_i \\ h_{23} - v_i \end{bmatrix} \tag{21}$$

APPENDIX B
CALIBRATION EXPERIMENT OF A 2D PROFILE SENSING SYSTEM

In this section, the procedure for calibrating the 2D profile sensing system is discussed. The target area was selected with respect to the printing area. The printing head of the 3D concrete printer has a rectangular nozzle with dimensions of 44 mm×11 mm (width× height). The camera calibration equipment consists of a camera and a calibration block made of aluminum. A checkerboard is attached to the block's surface where the 2D laser line is projected. The target area, measuring 70 mm × 35 mm, was selected based on the location of concrete filament extruded from the nozzle. This area contains of 98 squares (14 × 7) in alternating dark and light colors, each measuring 5 mm in width. The target area is indicated by a pink box, as shown in Fig. 19, and it includes 78 internal corner points (13 × 6).

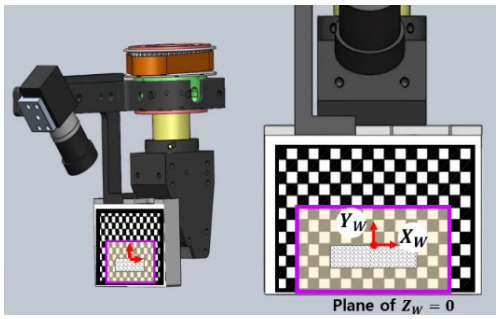

FIGURE 19. Camera calibration jig for a 2D profile sensing system.

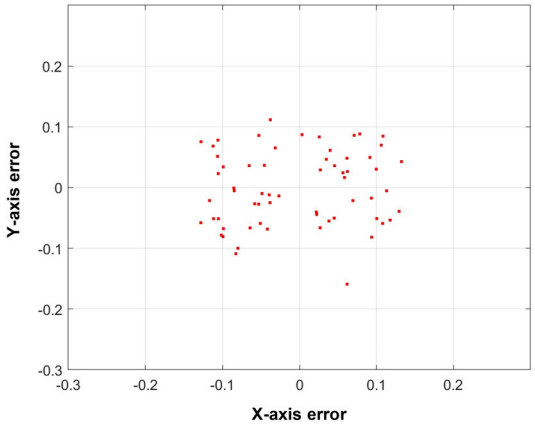

FIGURE 20. Spatial distribution of errors between measured points and theoretical points.

Calibration of a 2D laser profile sensor requires n points on the checkerboard (world coordinates) and their corresponding points in image coordinates. For corner points of the target area, OpenCV was used to collect the corresponding points in image coordinates. The image of the checkerboard was acquired using the camera from a 2D laser profile sensing system. A total of 78 corner points (u_i, v_i) were detected in the camera image. Using the corresponding information of world coordinate, the elements of the calibration parameter in the $\boldsymbol{h}$ vector were obtained using (19).

To verify the calibration performance, the world coordinates for all detected corner points (u_i, v_i) were calculated based on (21) and the obtained calibration vector $\boldsymbol{h}$. The MAE for the distance between the actual coordinates and the calculated world coordinates was 0.087 mm, with a standard deviation of 0.044 mm. The errors for the measured points were plotted in Fig. 20.

Besides, this article has a supplementary video material available at https://youtu.be/6ceaPdkufBk provided by the authors.

REFERENCES

[1] A. U. Rehman and J. H. Kim, "3D concrete printing: A systematic review of rheology, mix designs, mechanical, microstructural, and durability characteristics," *Materials*, vol. 14, no. 14, p. 3800, Jul. 2021.

[2] K. H. Jeon, M. B. Park, M. K. Kang, and J. H. Kim, "Development of an automated freeform construction system and its construction materials," in *Proc. Int. Symp. Autom. Robot. Constr. (ISARC)*, Montréal, QC, Canada, 2013, pp. 1359–1365.

[3] G. De Schutter, K. Lesage, V. Mechtcherine, V. N. Nerella, G. Habert, and I. Agusti-Juan, "Vision of 3D printing with concrete—Technical, economic and environmental potentials," *Cement Concrete Res.*, vol. 112, pp. 25–36, Oct. 2018.

[4] J. Chung, G. Lee, and J. H. Kim, "Framework for technical specifications of 3D concrete printers," *Autom. Concrete*, vol. 127, Jul. 2021, Art. no. 103732.

[5] R. J. M. Wolfs, T. A. M. Salet, and N. Roussel, "Filament geometry control in extrusion-based additive manufacturing of concrete: The good, the bad and the ugly," *Cement Concrete Res.*, vol. 150, Dec. 2021, Art. no. 106615.

[6] R. J. M. Wolfs and A. S. J. Suiker, "Structural failure during extrusion-based 3D printing processes," *Int. J. Adv. Manuf. Technol.*, vol. 104, pp. 565–584, Jun. 2019.

[7] M. K. Mohan, A. V. Rahul, G. De Schutter, and K. Van Tittelboom, "Extrusion-based concrete 3D printing from a material perspective: A state-of-the-art review," *Cement Concrete Compos.*, vol. 115, Jan. 2021, Art. no. 103855.

[8] A. Perrot, A. Pierre, V. N. Nerella, R. J. M. Wolfs, E. Keita, S. A. O. Nair, N. Neithalath, N. Roussel, and V. Mechtcherine, "From analytical methods to numerical simulations: A process engineering toolbox for 3D concrete printing," *Cement Concrete Compos.*, vol. 122, Sep. 2021, Art. no. 104164.

[9] A. Kazemian and B. Khoshnevis, "Real-time extrusion quality monitoring techniques for construction 3D printing," *Construct. Building Mater.*, vol. 303, Oct. 2021, Art. no. 124520.

[10] A. Kazemian, X. Yuan, E. Cochran, and B. Khoshnevis, "Cementitious materials for construction-scale 3D printing: Laboratory testing of fresh printing mixture," *Construct. Building Mater.*, vol. 145, pp. 639–647, Aug. 2017.

[11] A. U. Rehman, B. M. Birru, and J. H. Kim, "Set-on-demand 3D concrete printing (3DCP) construction and potential outcome of shotcrete accelerators on its hardened properties," *Case Stud. Construct. Mater.*, vol. 18, Jul. 2023, Art. no. e01955.

[12] R. J. M. Wolfs, F. P. Bos, E. C. F. van Strien, and T. A. M. Salet, "A real-time height measurement and feedback system for 3D concrete printing," in *High Tech Concrete: Where Technology and Engineering Meet*, D. Hordijk and M. Luković, Eds. Cham, Switzerland: Springer, 2018, pp. 2474–2483, doi: 10.1007/978-3-319-59471-2_282.

[13] J. Lee, "Realization of real-time height control in 3D concrete printing using depth sensor," M.S. thesis, Dept. Civil Environ. Eng., Yonsei Univ., Seoul, (South) Korea, 2020.

[14] A. Kazemian, X. Yuan, O. Davtalab, and B. Khoshnevis, "Computer vision for real-time extrusion quality monitoring and control in robotic construction," *Autom. Constr.*, vol. 101, pp. 92–98, May 2019.

[15] H. Lindemann, R. Gerbers, S. Ibrahim, F. Dietrich, E. Herrmann, K. Dröder, A. Raatz, and H. Kloft, "Development of a shotcrete 3D-printing (SC3DP) technology for additive manufacturing of reinforced freeform concrete structures," in *Proc. RILEM Int. Conf. Conc. Digit.*, Zurich, Switzerland, 2018, pp. 287–298.

[16] W. Huang and R. Kovacevic, "A laser-based vision system for weld quality inspection," *Sensors*, vol. 11, no. 1, pp. 506–521, Jan. 2011.

[17] X. Yang, O. Lakhal, A. Belarouci, and R. Merzouki, "Adaptive deposit compensation of construction materials in a 3D printing process," in *Proc. IEEE/ASME Int. Conf. Adv. Intell. Mechatronics (AIM)*, Sapporo, Japan, Jul. 2022, pp. 658–663.

[18] C. J. Ng and B. Farell, "Solving the stereo correspondence problem with false matches," *PLoS ONE*, vol. 14, no. 7, Jun. 2019, Art. no. e0219052.

[19] E. S. Barjuei, E. Courteille, D. Rangeard, F. Marie, and A. Perrot, "Real-time vision-based control of industrial manipulators for layer-width setting in concrete 3D printing applications," *Adv. Ind. Manuf. Eng.*, vol. 5, Nov. 2022, Art. no. 100094.

[20] J. Jhun, D. H. Lee, A. U. Rehman, and J. H. Kim, "Design of a real-time geometric quality monitoring system for 3D printed concrete filaments using 2D line laser," in *Proc. 4th Int. Conf. 3D Construction Printing (ICDP)*, Singapore, Jul. 2023, pp. 1–10.

[21] Z. Jin, Z. Zhang, X. Shao, and G. X. Gu, "Monitoring anomalies in 3D bioprinting with deep neural networks," *ACS Biomaterials Sci. Eng.*, vol. 8, no. 7, pp. 3945–3952, Jul. 2023.

[22] G. D. Goh, N. M. B. Hamzah, and W. Y. Yeong, "Anomaly detection in fused filament fabrication using machine learning," *3D Printing Additive Manuf.*, vol. 10, no. 3, pp. 428–437, Jun. 2023.

[23] Y. Fu, A. R. J. Downey, L. Yuan, and H. T. Huang, "Real-time structural validation for material extrusion additive manufacturing," *Additive Manuf.*, vol. 65, Mar. 2023, Art. no. 103409.
[24] G. L. Goh, G. D. Goh, J. W. Pan, P. S. P. Teng, and P. W. Kong, "Automated service height fault detection using computer vision and machine learning for badminton matches," *Sensors*, vol. 23, no. 24, p. 9759, Dec. 2023.
[25] D. Ding, W. Ding, R. Huang, Y. Fu, and F. Xu, "Research progress of laser triangulation on-machine measurement technology for complex surface: A review," *Measurement*, vol. 216, Jul. 2023, Art. no. 113001.
[26] Z. Zhang, "A flexible new technique for camera calibration," *IEEE Trans. Pattern Anal. Mach. Intell.*, vol. 22, no. 11, pp. 1330–1334, Nov. 2000.
[27] J. H. Kim, "Multi-axis force-torque sensor," in *Humanoid Robotics: A Reference*. Dordrecht, The Netherlands: Springer, 2018, doi: 10.1007/978-94-007-7194-9_104-1.
[28] X. Yang, X. Shen, J. Long, and H. Chen, "An improved median-based Otsu image thresholding algorithm," in *Proc. Conf. Model. Id. Cont. (MIC)*, Hong Kong, 2012, pp. 468–473.
[29] T. Cover and P. Hart, "Nearest neighbor pattern classification," *IEEE Trans. Inf. Theory*, vol. IT-13, no. 1, pp. 21–27, Jan. 1967, doi: 10.1109/TIT.1967.1053964.
[30] X. Xu, S. Xu, L. Jin, and E. Song, "Characteristic analysis of Otsu threshold and its applications," *Pattern Recognit. Lett.*, vol. 32, no. 7, pp. 956–961, May 2011.
[31] H. C. van Assen, M. Egmont-Petersen, and J. H. C. Reiber, "Accurate object localization in gray level images using the center of gravity measure: Accuracy versus precision," *IEEE Trans. Image Process.*, vol. 11, no. 12, pp. 1379–1384, Dec. 2002.
[32] *Scikit Learn. Sklearn.Linear_Model.LinearRegression*. Accessed: Feb. 10, 2023. [Online]. Available: https://scikit-learn.org/stable/modules/generated/sklearn.linear_model.LinearRegression.html
[33] A. U. Rehman, A. Perrot, B. M. Birru, and J. H. Kim, "Recommendations for quality control in industrial 3D concrete printing construction with mono-component concrete: A critical evaluation of ten test methods and the introduction of the performance index," *Devel. Built Env.*, vol. 16, Dec. 2023, Art. no. 100232.
[34] A. U. Rehman, I. K. Kim, and J. H. Kim, "Towards full automation in 3D concrete printing construction: Development of an automated and inline sensor-printer integrated instrument for in-situ assessment of structural build-up and quality of concrete," *Develop. Built Environ.*, vol. 17, Mar. 2024, Art. no. 100344.

JIHYE JHUN received the B.S. and M.S. degrees from the Department of Civil and Environmental Engineering, Yonsei University, Seoul, South Korea, in 2021 and 2023, respectively. She is currently pursuing the Ph.D. degree with the School of Mechanical and Aerospace Engineering, Nanyang Technological University, Singapore. Her research interests include 3D concrete printing technology, automation in construction, sensor development, quality monitoring in construction, and sustainable 3D concrete printing materials.

DONG-HYUN LEE received the B.S. degree in civil and environmental engineering from Yonsei University, Seoul, South Korea, in 2013, where he is currently pursuing the Ph.D. degree in civil and environmental engineering. His research interests include 3D concrete printing, structural analysis, and sensor development.

ATTA UR REHMAN received the Ph.D. degree in concrete structural engineering from Hanyang University, South Korea, in 2019. He is currently a Postdoctoral Researcher with the CORAL Lab, Department of Civil and Environmental Engineering, Yonsei University, Seoul, South Korea. He has expertise in 3D concrete printing construction, printable material development, print quality control, rheology of fresh concrete, structural analysis, and design.

SEUNGWOO KANG received the B.S. degree in civil and environmental engineering from Kookmin University, Seoul, South Korea, in 2022, and the M.S. degree in civil and environmental engineering from Yonsei University, Seoul, in 2024. His current research interests include 3D concrete printing technology, quality monitoring of construction, and developing smart equipment for construction.

JUNG-HOON KIM received the B.S. degree in mechanical design and production engineering from Yonsei University, Seoul, Republic of Korea, in 1997, and the M.S. and Ph.D. degrees in mechanical engineering from KAIST, in 1999 and 2004, respectively. From 2004 to 2005, he was a Postdoctoral Researcher with the Robotics and Human Engineering Laboratory, University of California at Berkeley. From 2005 to 2006, he was a Senior Engineer with the Mechatronics Center, Samsung Electronics. He is currently an Associate Professor with the Department of Civil and Environmental Engineering, Yonsei University. His research interests include 3D concrete printing technology, printable concrete, new sensing methods for digital concrete, automation in construction, sensors and actuators, machine learning applications, humanoid robots, and wearable exoskeleton robots. He is a member of American Concrete Institute (ACI), the International Union of Laboratories and Experts in Construction Materials, Systems and Structures (RILEM), Korea Robotics Society (KROS), and the Institute of Control, Robotics and Systems (ICROS).